

# Calibration of the STAR Forward Time Projection Chamber with Krypton-83m

V. Eckardt, T. Eggert, H. Fessler, H. Hümmeler, G. Lo Curto,  
M. Oldenburg, N. Schmitz, A. Schüttauf, J. Seyboth, P. Seyboth,  
M. Vidal

*Max-Planck-Institut für Physik, Föhringer Ring 6, 80805 München, Germany*

---

## Abstract

The principles of the calibration of a time projection chamber with radioactive Krypton-83 are explained. The calculation of gain correction factors and the methods of obtaining a precise energy calibration are illustrated. The properties and advantages of  $^{83m}\text{Kr}$  are summarized and compared to other radioactive calibration sources. It was shown that the Krypton calibration for the STAR FTPC is feasible and recommendable although the pad geometry of the FTPC causes a considerable deterioration of the measured spectrum due to only partially detected charge clusters.

---

The STAR experiment (Solenoidal Tracker at RHIC) is one of four experiments operating at the Relativistic Heavy Ion Collider (RHIC) in Brookhaven. STAR searches for hadronic signatures of the quark gluon plasma formation and investigates the behavior of strongly interacting matter at high energy density in collisions of heavy nuclei [1,2,3]. While the tracking in the central region is provided by a large TPC, the two Forward Time Projection Chambers (FTPCs) are required to give position, charge, and momentum information of particle tracks in the forward rapidity regions of the STAR experiment [4,5].

The calibration method using Krypton-83m has been developed by the ALEPH collaboration [6] and is being used by the DELPHI experiment [7]. It is also applied very successfully by the NA 49 experiment where the achieved measured accuracy (i. e. the relative error of the mean value  $\Delta E/E$ ) is better than 0.5 % [8].

## 1 The Calibration

A calibration of a Time Projection Chamber (TPC) is performed for two main purposes: The *gain correction*, which is needed to compensate variations in the front-

end electronics (FEE) and in the gas gain, and the *energy calibration*, which is performed in order to determine the amount of electric charge that is measured at a known energy deposition in the chamber.

### 1.1 Gain Correction

The gain of the pre-amplifier electronics varies from chip to chip (see also section 4) and within a chip from channel to channel. Moreover, variations in gas gain may occur due to inhomogeneities of the electric field and geometrical non-uniformities.

A straightforward and effortless relative gain correction for the pre-amplifier electronics can be performed by a so-called pulser calibration. This is done by injecting calibrated charge pulses into the anode or gating grid wires of the multi-wire proportional chambers (readout chambers). Each pulse induces a charge on each cathode pad  $i$ , resulting in a charge signal  $q_i$  which is proportional to the channel's response. Multiplicative calibration constants  $c_i$  are then obtained by dividing the average charge per pad

$$\bar{q} = \frac{1}{N} \sum_{i=1}^N q_i \quad (1)$$

( $N$  = number of pads) by the charge induced on an individual pad:

$$c_i = \frac{\bar{q}}{q_i} \quad (2)$$

Each measured charge per pad  $q_i^{\text{meas}}$  (i. e. integrated ADC channels) then gets multiplied by this calibration constant in order to obtain the calibrated charge:

$$q_i^{\text{cal}} = c_i q_i^{\text{meas}} \quad (3)$$

However, pulsing the anode wires induces a signal on all pads simultaneously, producing a large current load on each FEE channel which may result in a modification of the electronics response. Thus, the pulser calibration can only be considered as a first step in the calibration procedure.

### 1.2 Energy Calibration

It is not possible to perform an absolute energy calibration by a pulser calibration only. Therefore, an alternative calibration method using a radioactive source has to be considered. Although particle identification via  $dE/dx$  measurement is difficult

with the STAR FTPC [4, Sect. 6.6], an energy calibration is useful to optimize the accuracy of the position measurement. It can easily be done with a radioactive source such as  $^{83m}\text{Kr}$  which is injected into the chamber gas.

An electron emitted during the decay process of  $^{83m}\text{Kr}$  (see section 3) produces secondary electrons by ionization in the gas, where the number of produced electrons is proportional to the initial decay energy (i. e. the kinetic energy of the primary electron). Since the decay energies of suitable sources are relatively low ( $E \ll m_e c^2$ ), the primary electron is stopped very quickly, and the secondary electrons emerge from virtually one point. These secondary electrons are then drifted by an electric drift field to the readout chambers where they are amplified at the anode wires, and the charge signal from the gas amplification is detected at the cathode pads.

The decay energies of the radioactive source are known, and thus the corresponding energies can be assigned to the peaks of the measured charge spectra. Starting from a distinct reference peak, the energy that corresponds to a measured charge  $q$  is then calculated by

$$E(q) = q \frac{E_{\text{ref}}}{q_{\text{ref}}} \quad (4)$$

where  $E_{\text{ref}}$  is the energy and  $q_{\text{ref}}$  is the measured charge of the reference peak. However, because the highest decay energy of  $^{83m}\text{Kr}$  is relatively high compared to the energies of a few keV deposited by a minimum ionizing particle, the anode voltage  $U$  has to be reduced from the value suitable for minimum ionization. The results from the energy calibration must then be extrapolated to higher gain voltages. As the dependence of the amplification on the anode voltage has been measured, such an extrapolation is accurate.

Further applications of the Krypton calibration are a cross-check of the pulser calibration and an investigation of gas flow effects in the chamber by studying the location of Krypton decays at the beginning of the injection. Moreover, a calibration is needed to check the detector linearity over a wide energy range, and to monitor the long term detector stability.

## 2 The STAR Forward TPC

The high track density in the forward rapidity regions of the STAR experiment covered by the FTPCs (pseudorapidity range of  $2.5 < |\eta| < 4$ ) requires a special design for the tracking detectors in these regions. In contrast to conventional time projection chambers, the two Forward TPCs of the STAR detector use radial drift fields, and the curved readout chambers are part of the outer cylinder walls. The compactness of the FTPCs (60 cm diameter and 120 cm length) with only 22 cm

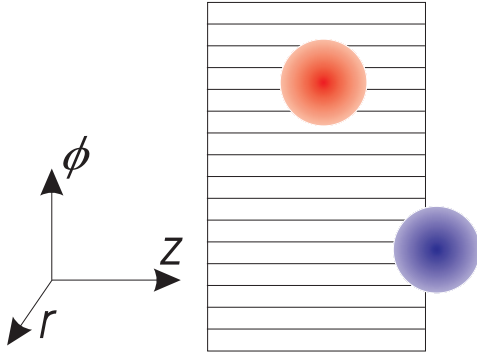


Fig. 1. Two electron clusters produced by Krypton decays and a row of cathode pads. As the padrows are not adjacent to each other, for some of the clusters the charge can only be partially detected [9].

drift length and the use of a cool gas provides a very good position resolution ( $150 \mu\text{m}$ ) and two-track separation ( $1 \text{ mm}$ ) [9,10]. In order to minimize the number of readout channels without compromising the detector performance the surface is covered only partially by cathode pads. There are 10 padrows per FTPC, with 960 pads each. The length of one pad is  $20 \text{ mm}$  (in  $z$  direction, where  $z$  points along the beam pipe), and the pad pitch is  $1.9 \text{ mm}$  (in azimuthal direction  $\phi$ ). The distance between the padrows is intermittently  $65 \text{ mm}$  and  $85 \text{ mm}$ . For further details on the STAR FTPC, see [4,5].

As the padrows are not adjacent to each other, a problem arises when localized charge clusters from radioactive decays are to be detected. As illustrated in figure 1, only a fraction of the cluster charge can be detected by the pads when the cluster is located at the border of a padrow. The question whether a calibration with a radioactive source can nevertheless be done triggered a systematic investigation on the practicability of a calibration with radioactive Krypton.

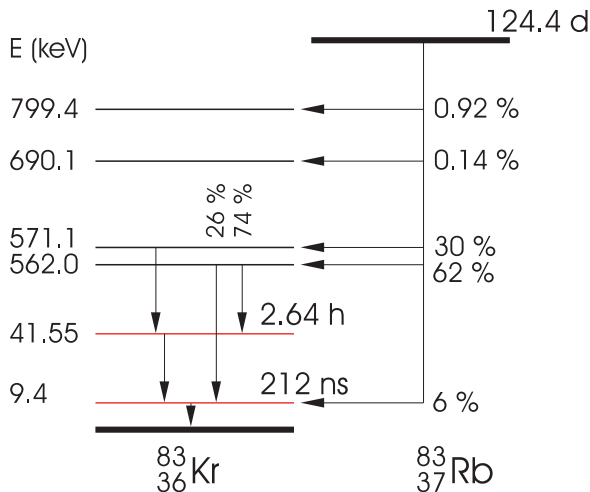


Fig. 2. Decay scheme of  $^{83}\text{Rb} \rightarrow ^{83}\text{Kr}$ . The ground state of  $^{83}\text{Rb}$  decays predominantly (76%) to the isomeric excited state  $^{83m}\text{Kr}$  at  $E = 41.6 \text{ keV}$ . This most important level of  $^{83}\text{Kr}$  for calibration is populated through the 571 keV and 562 keV intermediate levels. It decays entirely to the 9.4 keV state, which then decays to the  $^{83}\text{Kr}$  ground state.

### 3 Properties of Krypton-83

$^{83}\text{Kr}$  is a stable isotope produced from  $^{83}\text{Rb}$  which decays by electron capture with a mean lifetime of 124 days. The decay scheme [11] is shown in figure 2. The ground state of  $^{83}\text{Kr}$  is not reached directly in the  $^{83}\text{Rb}$  decay but via nuclear transitions from intermediate excited  $^{83}\text{Kr}$  levels. The relevant level for drift chamber calibration is the isomeric (metastable) 41.6 keV state  $^{83m}\text{Kr}$ . It is fed down from two higher  $^{83}\text{Kr}$  levels in 76 % of all  $^{83}\text{Rb}$  decays and has a lifetime long enough ( $\tau = 2.64\text{ h}$ ) for the  $^{83m}\text{Kr}$  to be introduced and distributed in the drift chamber before it decays. The isomeric state  $^{83m}\text{Kr}$  decays entirely by an E3 nuclear de-excitation transition to the 9.4 keV level with a transition energy  $E_{\text{tr}}$  of 32.2 keV. This short-lived state then decays immediately ( $\tau = 212\text{ ns}$ ) to the  $^{83}\text{Kr}$  ground state with  $E_{\text{tr}} = 9.4\text{ keV}$ . In contrast to other common calibration sources like  $^{55}\text{Fe}$  or  $^{57}\text{Co}$ , almost no low energy photons are produced since both transitions from the 41.6 keV and the 9.4 keV states proceed almost entirely by internal conversion (IC) with ratios of electron-to-photon emission of  $e^-/\gamma \approx 2 \cdot 10^3$  and  $e^-/\gamma \approx 20$  respectively.

The kinetic energy  $E_e$  of an IC electron is given by

$$E_e = E_{\text{tr}} - E_b \quad (5)$$

where  $E_b$  is the atomic binding energy of the electron. The subsequent atomic de-excitation of the electron hole produces either X-rays or Auger electrons with an energy equal to  $E_b$ .

For the 41.6 keV-to-9.4 keV transition the internal  $\gamma$  conversion occurs predominantly on an electron in an outer (L, M, N) shell, the total electron emission probability from such shells being 77 % [11]. The binding energies for the outer shells are small ( $E_b \leq 1.9\text{ keV}$ ). Furthermore, the de-excitation of an outer-shell hole leads in most cases to the emission of an Auger electron rather than an X-ray. Therefore practically the full energy  $E_{\text{tr}}$  of 32.2 keV is carried away by electrons and can be collected. If, however, the internal conversion occurs in the K shell (23 % of the cases) an IC electron with an energy  $E_e$  of 17.8, 18.1, 19.5 or 19.6 keV is produced, corresponding to four K sub-levels with binding energies of 14.3, 14.1, 12.7 and 12.6 keV [11], respectively, according to eq. (5). In addition, the de-excitation of the K-shell hole yields X-rays or Auger electrons with an energy equal to the binding energy.

For the 9.4 keV-to-ground state transition the low transition energy allows only internal conversion on an outer-shell electron, so that practically the full transition energy of 9.4 keV is carried away by the IC electron (95 % of the cases) or by the escaping  $\gamma$  (5 %).

For more details on the released energies and on the branching fractions, see [11].

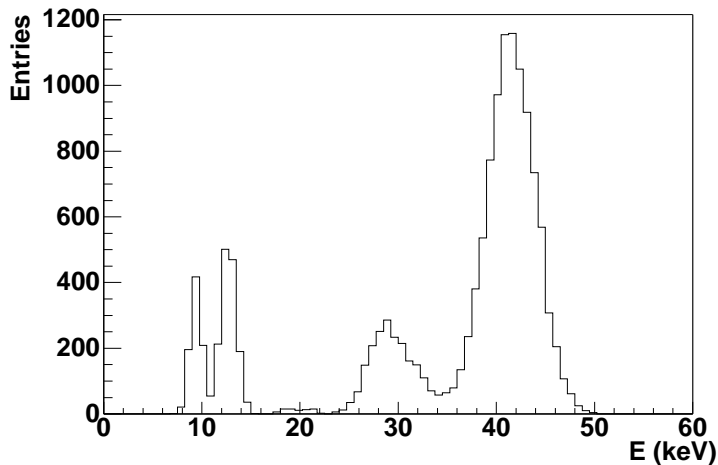


Fig. 3. Simulated decay spectrum of  $^{83m}\text{Kr}$  with an assumed line width of  $\sigma/E = 6\%$ . Noise is neglected.

The overall decay spectrum has been simulated, using the branching fractions in table 4 of [11] and assuming a resolution of  $\sigma/E = 6\%$ , where  $\sigma$  is the width of a Gaussian. The simulated spectrum is shown in figure 3; it is composed of five parts:

- The strong peak at 41.6 keV is due to the electrons from the dominant modes of the two-step decay of the 41.6 keV isomeric state via the 9.4 keV state. Because of the short lifetime of the 9.4 keV state the two decay energies of 32.2 keV and 9.4 keV are deposited in the majority of cases at the same location such that the total decay energy is collected in a single cluster.
- The smaller peak around 30 keV comes from two contributions: (a) electrons with  $E_e = 32.2$  keV from the 41.6 keV-to-9.4 keV transition when the 9.4 keV  $\gamma$  escapes; (b) K-shell IC electrons ( $E_e \approx 19.5$  keV) together with IC electrons from the decay of the 9.4 keV state at the same location, leading to a total energy deposition of  $\sim 29$  keV.
- The very small accumulation around 20 keV is due to K-shell IC electrons ( $E_e \approx 19.5$  keV) when the 9.4 keV  $\gamma$  escapes.
- The peak at 12.7 keV is produced by the conversion of K-shell X-rays in the chamber gas, away from the location of their origin.
- The peak at 9.4 keV results from either the conversion of the escaped 9.4 keV  $\gamma$  in the gas or the 9.4 keV electron energy, separated from the preceding 32.2 keV transition.

Figure 4 shows a more detailed simulation, where partially detected clusters caused by the pad geometry, diffusion, the detector resolution, and cut criteria comparable to those in the experiment were considered. The 41.6 keV peak is clearly visible while the several peaks around 30 keV as well as the 9.4 keV and the 12.7 keV peaks are hardly separable. Moreover, the shape of the low energy part of the spectrum is strongly affected by the chosen threshold.

The isomeric state  $^{83m}\text{Kr}$  is a very useful isotope for calibrating a time projection chamber for several reasons: in contrast to other frequently used calibration sources

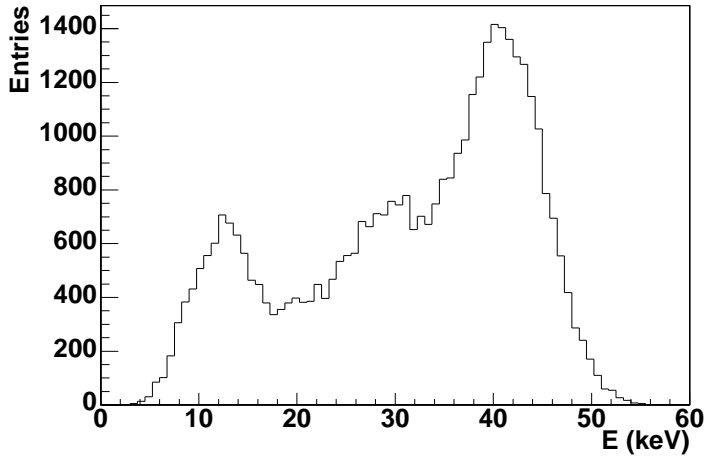


Fig. 4. Simulation of the  $^{83m}\text{Kr}$  decay spectrum as seen by the two padrows of the test-setup. Diffusion, partially detected clusters, and a threshold cut are taken into account.

such as  $^{55}\text{Fe}$ ,  $^{83}\text{Kr}$  is a gas which can be distributed over the chamber volume using the existing gas system. Therefore, no laborious unmounting of the chamber and installation of Fe sources is necessary. The mean lifetime of  $^{83m}\text{Kr}$  is short enough to ensure the chamber to operate normally again after a reasonably short time, i. e. once a few half-lives have passed after cutting off the Krypton supply to the chamber. If required, the gas can be left within the closed gas system until the radioactivity subsides. On the other hand, the mean lifetime of the isomeric state is long enough for a sufficient number of subsequent decays to occur inside the chamber. Krypton's parent isotope  $^{83}\text{Rb}$  has a sufficiently long mean lifetime ( $\tau = 124\text{d}$ ), is a solid, and thus may be mounted as a foil inside a bypass line of the gas system.

As it is not possible to trigger on the Krypton decays, a random trigger must be used. The decay rate must be high enough to ensure good statistics within a reasonable time (an estimate of the number of events needed is carried out at the end of section 4). Due to random triggering there is no information on the decay position in the drift direction. Therefore, to obtain a clean spectrum, absorption (mainly caused by oxygen pollution in the gas) must be small<sup>1</sup>.

#### 4 The Measurements

As neither the STAR FTPC nor the FTPC readout electronics were completed when the measurements were performed, a small test-setup using the NA 49 readout electronics [12,13] was constructed. For this test-setup, the same materials and gas-mixture (Ar/CO<sub>2</sub> 50/50) as for the FTPC, and a pad geometry comparable to the FTPC (two non-adjacent padrows with 16 pads each) were used. The major differ-

<sup>1</sup> At an oxygen concentration of 5 ppm and the maximum drift time of  $50\ \mu\text{s}$ , 17 % of the electrons are absorbed [14].

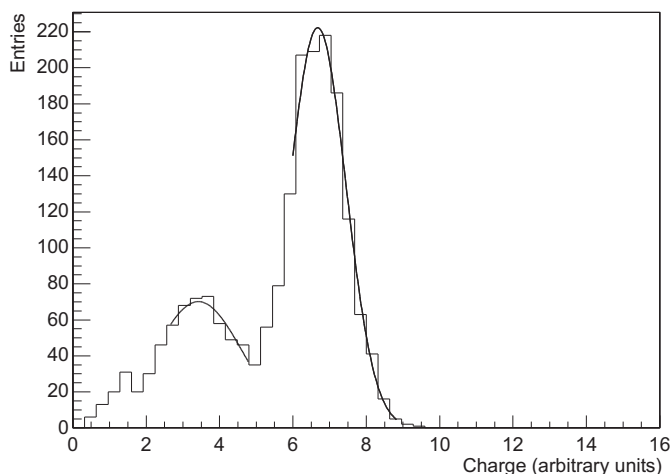


Fig. 5. A Fe spectrum measured on a single pad. A combined fit consisting of two Gaussians was performed and the two separate Gaussians are shown in this plot.

ences between the test-setup and the FTPC was the axial drift field (in contrast to the radial drift field of the FTPC) and the planar readout chamber. However, the charge deposited on the pads is hardly affected by the drift field geometry and the cluster sizes were comparable to those measured in a test TPC with a radial drift field. For details on the test-setup and the measurements, see [14].

The calibration was performed in three steps: the pulser calibration, the calibration with  $^{55}\text{Fe}$ , and the calibration with  $^{83m}\text{Kr}$ .

#### 4.1 The Preparatory Calibrations

The pulser calibration is described earlier in section 1.1. The amplification factors of the 16 channels per preamplifier/shaper chip decrease characteristically with increasing channel number  $i$ ; they differ by up to 15 %. This behavior is a property of the architecture of the NA 49 FEE chips and is not observed in the FTPC electronics where the fluctuation of the amplification factor is below 3 %. Thus, a pad-wise calibration was necessary for the test-setup but might not be needed for the calibration of the FTPC. However, the pulse shape of the FTPC electronics is affected by the current load on the chip. The rise time of the pulse is reduced as the number of pulsed channels increases [15] which will affect the total integrated cluster charge. Thus, a cross-check of the pulser calibration has to be performed.

For the measurements with the  $^{55}\text{Fe}$  source, two Aluminum strips doped with  $^{55}\text{Fe}$  were mounted at the cathode plate of the drift field cage, opposite to the two pad-rows.  $^{55}\text{Fe}$  decays via electron capture to  $^{55}\text{Mn}$  which subsequently emits an X-ray photon from the K-shell with an energy of 6 keV. This photon may ionize an Argon atom in the gas which releases an electron from the K-shell, which has a binding energy of 3.2 keV. In addition, either Auger electrons or an escaping X-ray photon with an energy of 3.2 keV are emitted, the latter being responsible for the



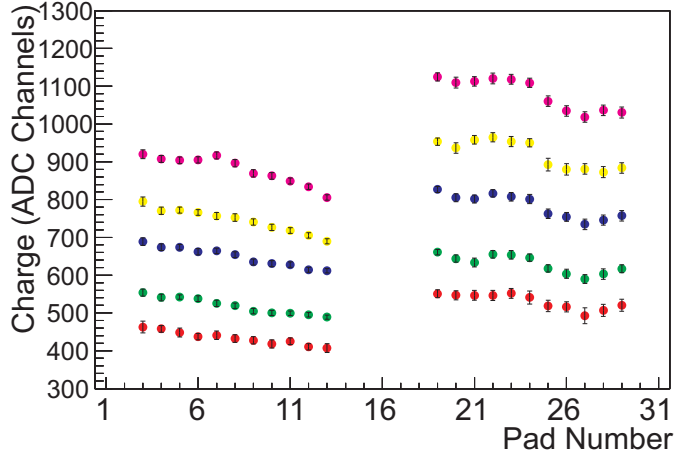


Fig. 6. The measured charge  $q_i$  (integrated ADC channels) from the 6 keV Fe decays of each pad  $i$  without any calibration. Anode voltages from the bottom up:  $U = 1700$  V, 1725 V, 1750 V, 1775 V, 1800 V.

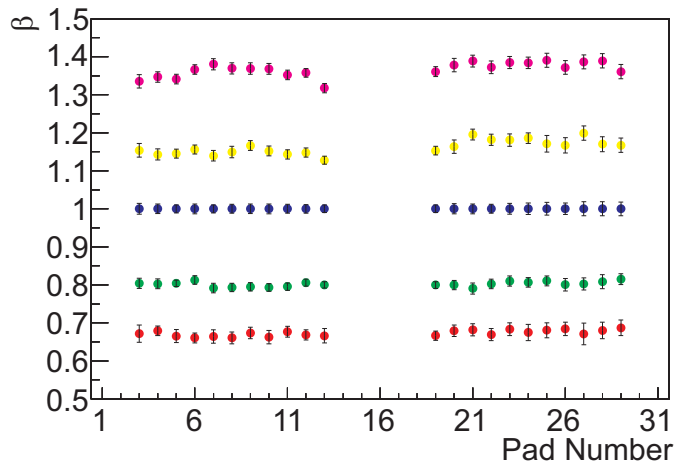


Fig. 7. The measured charge  $q_i$  from Fe decays of each pad  $i$  (as in fig. 6) with calibration factors obtained by the reference measurement at 1750 V.  $\beta = q_i(U)/q_i(1750 \text{ V})$

2.8 keV escape peak [14]. The supplementary calibration using  $^{55}\text{Fe}$  was performed for several reasons:

- A cross-check of the pulser calibration and a first order energy calibration was needed to tune the anode voltage for the Krypton measurements.
- Determining the widths of the 6 keV main peak and of the 3 keV escape peak gave an accurate measurement of the chamber resolution.
- A comparison of the gas amplification at anode voltages in the operating range of the FTPC (1700 V to 1800 V) was required.
- The clear Fe spectrum allowed a straightforward determination of suitable cut criteria in order to reduce noise.

The electron energy deposition of  $^{55}\text{Fe}$  roughly corresponds to the energy deposition of a minimally ionizing particle. Thus, it was possible to perform an energy calibration at the FTPC's operating anode voltage of  $U = 1750$  V. In addition, further measurements at voltages from 1700 V to 1800 V were carried out. These results were extrapolated to lower voltages in order to find the anode voltage where the complete Krypton spectrum can be measured without electronics saturation caused by the high decay energies of  $^{83m}\text{Kr}$ .

For each pad a separate Fe spectrum was measured and a combined fit of the two peaks was performed (see figure 5). For the calculation of the calibration factors only the position of the 6 keV peak was considered. The width of the peak and hence the detector resolution were determined to be  $\sigma/E \approx 12\%$ . The positions of the fitted Gaussians on the charge spectra of each pad (except the marginal pads) is shown as a function of the pad number in figure 6. By applying the Fe calibration factors from a reference measurement at 1 750 V to measurements at different anode voltages, the consistency of the Fe calibration and thus the expected precision for the Krypton calibration was investigated (see figure 7, where only statistical errors are shown). The resulting uncertainty is determined to be  $< 2\%$ .

The comparison of the calibration factors obtained with the pulser and the iron source shows notable differences. The drop in amplification with increasing channel number is smaller for calibration using the Fe source ( $\lesssim 11\%$ ) than for the pulser calibration ( $\lesssim 15\%$ ). This is due to the lower current demand of the amplifying electronics in the case of the Fe measurement because only a few pads receive charge signals.

A thorough investigation of cut criteria showed that constraints on the cluster size in drift direction  $r$  and in  $\phi$  direction (see coordinate system in figure 1) significantly improve the spectra and reduce noise and background. An effective background rejection is of great importance for the following calibration with  $^{83m}\text{Kr}$ . Moreover, clusters located at the marginal pads of each padrow were rejected.

## 4.2 The Krypton Calibration

In the first step, Krypton spectra were recorded at high anode voltages (1 600 V and 1 700 V), focusing on the 9.4 keV peak. The calibration factors from the Fe reference measurement were applied to the data and the spectra from the individual pads were combined to one spectrum. By this means, the accuracy of the extrapolation of the gas gain measurements with Fe from high anode voltages to lower voltages was checked. This extrapolation was correct within an error  $< 3\%$ , which includes statistical and systematical errors. The optimum anode voltage for collecting the complete Krypton spectrum was determined to be 1 500 V.

In the second step, a high statistics run at 1 500 V was carried out in order to allow a pad-wise calibration with the 41.6 keV peak. In some of the high energy decays, several electrons are produced consecutively in a short time span. This results in charge clusters with multiple peaks. As the summed electron energy is relevant, a special cluster finder<sup>2</sup> was used that does not deconvolute overlapping clusters, but sums up the total charge.

<sup>2</sup> The cluster finder calculates the charge and other parameters like position and width of each found cluster from the raw data.

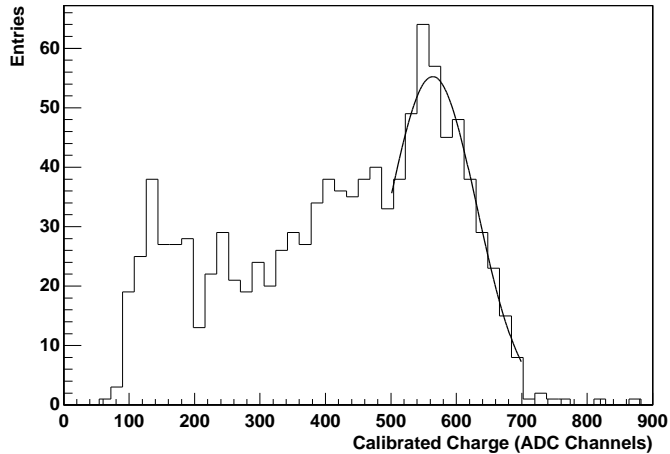


Fig. 8. Krypton spectrum of a single pad at an anode voltage of 1500 V. At higher anode voltages, only the low energy part of the spectrum can be detected.

The cuts determined by the Fe measurements were applied and the calibration constants were then obtained by fitting a simple Gaussian to the upper part of each spectrum (see figure 8). This calibration was repeated iteratively several times since the cluster charge is summed up from several pads with different calibration factors although the resulting charge is assigned to the spectrum of the central pad.

Finally, a total Krypton spectrum was obtained by combining the calibrated spectra of the single pads (except the marginal pads). This measured Krypton spectrum is in good agreement with the simulation (compare figures 4 and 9). The position of the peaks were determined by a combined fit to a satisfactory precision. Both the linearity and the accuracy of the fitting procedure were checked in the following way: The maximum of the high energy peak was assigned to an energy of 41.6 keV. The energies of the other peaks were then calculated from their fitted positions, assuming linearity. The deviations of the energies thus obtained from the expected values were  $\approx 2\%$ . The relative width  $\sigma/E$  of the 41.6 keV peak (i. e. the resolution) was determined to be 10 %.

The amplification in the gas is sensitive to the density which changes due to temperature and atmospheric pressure variations. Therefore the measurements were performed in an air-conditioned room. As the atmospheric pressure was not monitored during the measurements, a more precise calibration can be attained when appropriate correction factors are applied to the data.

In order to obtain a spectrum where the 41.6 keV peak can be fitted precisely, at least 1 000 decay events that fulfill the cut criteria are required. With moderate cut criteria, 80 % of the events pass the cuts and thus 1 250 events have to be recorded. Consequently, if a pad-wise calibration of the FTPC's 19 200 pads is required, a total of  $24 \cdot 10^6$  events is needed. For a chip-wise calibration (each chip reads out 16 pads) this number decreases to  $1.5 \cdot 10^6$  events. Assuming that the data can be written with a rate of 15 Hz and that there is one Krypton decay detected per trigger, it takes about 28 hours to record  $1.5 \cdot 10^6$  events.

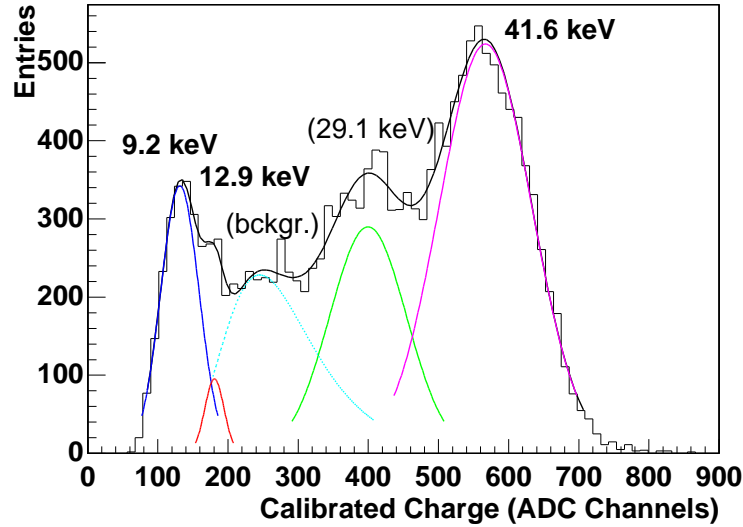


Fig. 9. The measured Krypton spectrum of all pads calibrated with the calibration constants obtained from the Krypton spectra of the single pads. A combined fit using 4 Gaussians for the peaks (solid grey lines) and one Landau distribution for the background (dotted line) was performed. The maximum of the high energy peak was assigned an energy of 41.6 keV and thus the energies of the other peaks were calculated (see values at the various peaks).

## 5 Conclusions

It was shown that a calibration with Krypton-83m is a very useful and convenient calibration method for the STAR FTPC. Its practicability is not affected by the FTPC's pad geometry where the cathode is not completely covered with pads. With this method, both a compensation of deviations in amplification within 2 % and a precise energy calibration can be obtained. The energy resolution was determined to be  $\sigma/E = 10\%$ .

## References

- [1] STAR Collaboration, Conceptual Design Report for the Solenoidal Tracker at RHIC, *LBL/PUB-5347*, 1992
- [2] J. W. Harris et al., The STAR Experiment at the Relativistic Heavy Ion Collider, *Nucl. Phys. A* **566** (1994) 277c
- [3] H. Wieman et al., Recent Developments on the STAR Detector System at RHIC, *Nucl. Phys. A* **638** (1998) 559c
- [4] The STAR FTPC Collaboration, Proposal for the Forward Time Projection Chamber for the STAR Detector, *MPI PhE/98-3*, 1998

- [5] A. Schüttauf et al., A Forward TPC for STAR, *Nucl. Phys. A* **661** (1999) 677c
- [6] D. Decamp et al., ALEPH – A Detector for Electron Positron Annihilation at LEP, *Nucl. Instr. Meth. A* **294** (1990) 121
- [7] A. Chan et al., Performance of the HPC Calorimeter in DELPHI, *IEEE Trans. Nucl. Sci.* **42** (1995) 491
- [8] S. Afanasiev et al., The NA 49 Large Acceptance Hadron Detector, *Nucl. Instr. Meth. A* **430** (1999) 210
- [9] R. Marsteller, Diploma Thesis, Technical University, München, Germany, 1998
- [10] H. Hümmeler, Doctorate Thesis, Technical University, München, Germany, 2000
- [11] B. Lasiuk, C. A. Whitten, Use of Krypton-83 as a Calibration Source for the STAR TPC, *STAR Note 360*, 1998
- [12] W. Rauch et al., The NA 49 Data Acquisition System, *IEEE Trans. Nucl. Sci.* **41**, 1994
- [13] F. Bieser et al., Design and Performance of TPC Readout Electronics for the NA 49 experiment, *Nucl. Instr. Meth. A* **385** (1997) 535
- [14] T. Eggert, Diploma Thesis, Technical University, München, Germany, 2000
- [15] B. Lasiuk, Investigation of the STAR FEE Response to the FEE Pulser at the TPC System Test, *STAR Note 324*, 1998